

A molecular-dynamics approach for studying thermalization properties of x-ray-heated solid-density matter

Malik Muhammad Abdullah,^{1,2,3} Anurag,^{4,1} Zoltan

Jurek,^{1,2} Sang-Kil Son,^{1,2} and Robin Santra^{1,2,3}

¹*Center for Free-Electron Laser Science, DESY,
Notkestrasse 85, 22607 Hamburg, Germany*

²*The Hamburg Centre for Ultrafast Imaging,
Luruper Chaussee 149, 22761 Hamburg, Germany*

³*Department of Physics, University of Hamburg,
Jungiusstrasse 9, 20355 Hamburg, Germany*

⁴*Department of Physics, Indian Institute of Technology, Kharagpur, West Bengal, India*

(Dated: November 18, 2018)

Abstract

When matter is exposed to a high-intensity x-ray free-electron-laser pulse, the x rays excite inner-shell electrons leading to the ionization of the electrons through various atomic processes and creating high-energy-density plasma, i.e., warm dense matter. The resulting system consists of atoms in various electronic configurations, thermalizing on sub-picosecond to picosecond timescales after photoexcitation. We present a simulation study of x-ray-heated warm dense matter. For this we use XMDYN, a Monte-Carlo molecular-dynamics-based code with periodic boundary conditions, which allows one to investigate non-equilibrium dynamics and in particular, the approach to equilibrium. XMDYN is capable of treating systems containing light and heavy atomic species with full electronic configuration space and 3D spatial inhomogeneity. We compare the electron temperatures and the ion charge-state distribution from XMDYN to results on the thermalized system based on the average-atom model implemented in XATOM, an *ab-initio* x-ray atomic physics toolkit extended to include a plasma environment. Further, we also compare average charge evolution for a system reaching towards equilibrium with the predictions of a Boltzmann continuum approach. We demonstrate that XMDYN results are in good quantitative agreement with the above mentioned approaches, suggesting that the current implementation of XMDYN is a viable approach to simulate the dynamics of x-ray-driven matter.

I. INTRODUCTION

X-ray free-electron lasers (XFELs) [1, 2] provide intense radiation with a pulse duration down to only tens of femtoseconds. The cross sections for the elementary atomic processes during x-ray-matter interactions are small. Delivering high x-ray fluence can increase the probabilities of photoionization processes to saturation [3]. Nonlinear phenomena arise because of the complex multiphoton ionization pathways within molecular or dense plasma environment [4–8]. Theory has a key role in revealing the importance of different mechanisms in the dynamics. Many models have been developed for this purpose using both particle and continuum approaches [9–11]. In order to give a complete description of the evolution of the atomic states in the plasma, one needs to account for the possible occurrence of all electronic configurations of the atoms/ions. A computationally demanding situation arises when a plasma consists of heavy atomic species [12, 13]. For example at a photon energy of 5.5 keV, the number of electronic configurations accessible in a heavy atom such as Xenon ($Z=54$) is about 20 million [13]. If one wants to describe the accessible configuration space of two such atoms, one must deal with $(2 \times 10^7)^2 = 4 \times 10^{14}$ electronic configurations. It is clear that following the populations of all electronic configurations in a polyatomic system as a function of time is a formidable task. To avoid this problem, there have been models that use a set of average configurations [14, 15] or limit the available configurations by using a pre-selected subset of configurations in predominant relaxation paths [16].

The most promising approach to address this challenge is to sample the most important pathways in the unrestricted polyatomic electronic configuration space. This can be realized by using a Monte-Carlo strategy, which is straightforward to implement in a particle approach. In our study we simulate the effect of individual ultrafast XFEL pulses [17–23] of different intensities incident on a model system of carbon atoms placed on a lattice and analyze the equilibrium plasma state of the material reached through ionization and thermalization. In order to have a more comprehensive description during thermalization we include all possible atomic electron configurations for Monte-Carlo sampling, and no pre-selection of transitions and configurations is introduced. To this end, we use two different tools. One is XMDYN [7, 8, 24], a Monte-Carlo molecular-dynamics based code, and the other is an average-atom model implemented within the XATOM code [25].

XMDYN gives a microscopic description of a polyatomic system, and phenomena such

as sequential multiphoton ionization [3, 12, 26], nanoplasma formation [8], thermalization of electrons through collisions and thermal emission [8] emerge as an outcome of a simulation. Probabilities of transitions between atomic states are determined by cross-section and rate data that are calculated by XATOM [24, 27, 28], a toolkit for x-ray atomic physics. In XMDYN individual ionization and relaxation paths are generated via a Monte-Carlo algorithm. A recent extension of XMDYN to periodic boundary conditions allows us to investigate bulk systems [29, 30].

The other approach we use is a warm-dense-matter simulation extension of XATOM to an average-atom model (AA) [25], which gives a statistical description of the behavior of atoms immersed in a plasma environment. It calculates plasma properties such as ion charge-state populations and plasma electron densities for a system with a given temperature. We compare the electron temperatures and ion charge-state distributions provided by XMDYN and AA.

Finally, we make a comparison between predictions for thermalization dynamics in irradiated diamond obtained by the XMDYN particle approach and results from a Boltzmann continuum approach published recently [16]. With these comparisons, we demonstrate the potential of the XMDYN code for the description of high-energy-density bulk systems in and out of equilibrium.

II. THEORETICAL BACKGROUND

A. XMDYN: Molecular dynamics with super-cell approach

XMDYN [24] is a computational tool to simulate the dynamics of matter exposed to high-intensity x rays. A hybrid atomistic approach [19, 24] is applied where neutral atoms, atomic ions and ionized (free) electrons are treated as classical particles, with defined position and velocity vectors, charge and mass. The molecular-dynamics (MD) technique is applied to calculate the real-space dynamics of these particles by solving the classical equations of motion numerically. The electrons bound to ions or neutral atoms are considered to be in discrete atomic quantum energy states. XMDYN keeps track of the electronic configuration of all the atoms and atomic ions. XMDYN calls the XATOM toolkit on the fly, which provides rate and cross-section data of x-ray-induced processes such as photoioniza-

tion, Auger decay, and x-ray fluorescence, for all possible electronic configurations accessible during intense x-ray exposure. Probabilities derived from these parameters are then used in a Monte-Carlo algorithm to generate a realization of the stochastic inner-shell dynamics. XMDYN includes secondary (collisional) ionization and recombination, the two most important processes occurring due to an environment. XMDYN has been validated quantitatively against experimental data on finite samples calculated within open boundary conditions [7, 8].

Our focus here is the bulk properties of highly excited matter. XMDYN uses the concept of periodic boundary condition (PBC) to simulate bulk behavior [29, 30]. In the PBC concept, we calculate the irradiation-induced dynamics of a smaller unit, called a super-cell. A hypothetical, infinitely extended system is constructed as a periodic extension of the super-cell. The driving force of the dynamics, the Coulomb interaction, is then calculated for all the particles inside the super-cell within the minimum image convention [31]. Therefore, the total Coulomb force acting on a charge is given by the interaction with other charges within its well-defined neighborhood containing also particles of the surrounding copies of the super-cell.

B. XMDYN: Impact ionization and recombination

While core excited states of atoms decay typically within a few tens of femtoseconds, electron impact ionization and recombination events occur throughout the thermalization process and are in dynamical balance in thermal equilibrium. Here we disregard energy loss due to fluorescence. The models used in this study consider these processes on different footage that we overview in this section. Within the XMDYN particle approach, electron impact ionization is not a stochastic process (i.e., no random number is needed in the algorithm), but it depends solely on the real space dynamics (spatial location and velocity) of the particles and on the cross-section. When a classical free electron is close to an atom/ion, its trajectory is extrapolated back to an infinite distance in the potential of the target ion by using energy and angular momentum conservation. Impact ionization occurs only if the impact parameter at infinity is smaller than the radius associated with the total electron impact ionization cross section. The total cross section is a sum of partial cross sections evaluated for the occupied orbitals, using the asymptotic kinetic energy of the impact electron. In

the case of an ionization event the orbital to be ionized is chosen randomly, according to probabilities proportional to the subshell partial cross sections. XMDYN uses the binary-encounter-Bethe (BEB) cross sections [32] supplied with atomic parameters calculated with XATOM. Similarly in XMDYN recombination is a process that evolves through the classical dynamics of the particles. It checks for the ion that has the strongest Coulomb potential for each electron and calculates for how long this condition is fulfilled. Recombination occurs when an electron remains around the same ion for n full periods (e.g., $n = 1$) [33]. While recombination can be identified based on this definition, the electron is still kept classical if its classical orbital energy is higher than the orbital energy of the highest considered orbital i containing a vacancy. When the classical binding becomes stronger, the classical electron is removed and the occupation number of the corresponding orbital is incremented by one.

C. XMDYN: Electron plasma analysis

Electron plasma is formed when electrons are ejected from atoms in ionization events and stay among the ions through an extensive period, e.g. in a bulk. The plasma dynamics are governed by not only the Coulomb interaction between the particles but also by collisional ionization, recombination, and so on. XMDYN follows the system from the very first photoionization event through non-equilibrium states until thermalization is reached asymptotically. In order to quantify the equilibrium properties reached, we fit the plasma electron velocity distribution using a Maxwell-Boltzmann distribution,

$$f(v) = \sqrt{\left(\frac{1}{2\pi T}\right)^3} 4\pi v^2 e^{-\frac{v^2}{2T}}, \quad (1)$$

where T represents the temperature (in units of energy), and v is the electron velocity. Atomic units are used unless specified. With the function defined in Eq. (1) we fit the temperature, which is used later to compare with equilibrium-state calculations.

D. Average-atom model

The average-atom model (AA) uses a finite-temperature Hartree-Fock-Slater calculation, which is implemented as an extension of XATOM [25]. AA corresponds to the first step of the two-step model that was used to describe ionization potential depression in dense

plasmas [25]. For a single atomic species, the effect of the solid/plasma environment on an electron is taken into account via a muffin-tin-type potential given as

$$V(\mathbf{r}) = \begin{cases} -\frac{Z}{r} + \int_{r' \leq r_s} d^3r' \frac{\rho(\mathbf{r}')}{|\mathbf{r}-\mathbf{r}'|} - \frac{3}{2} \left[\frac{3}{\pi} \rho(\mathbf{r}) \right]^{\frac{1}{3}} & \text{for } r \leq r_s \\ V(r_s) & \text{for } r > r_s, \end{cases} \quad (2)$$

where Z is the nuclear charge, $\rho(\mathbf{r})$ is the electronic density, and r_s is the Wigner-Seitz radius that is given by the number density n_i of the atomic ions in the solid, using the expression $r_s = (3/4\pi n_i)^{\frac{1}{3}}$. Using this potential we solve the effective single-electron Schrödinger equation,

$$\left[-\frac{1}{2} \nabla^2 + V(\mathbf{r}) \right] \psi_p(\mathbf{r}) = \varepsilon_p \psi_p(\mathbf{r}), \quad (3)$$

where p is a one-particle state index and ε_p is the corresponding orbital energy. The average-atom calculation treats the electronic system using a grand-canonical ensemble. The electronic density then becomes

$$\rho(\mathbf{r}, T) = \sum_p |\psi_p(\mathbf{r})|^2 \tilde{n}_p(\mu, T). \quad (4)$$

Here $\tilde{n}(\mu, T)$ stands for the fractional occupation numbers given by the Fermi-Dirac distribution at chemical potential μ ,

$$\tilde{n}_p(\mu, T) = \frac{1}{e^{(\varepsilon_p - \mu)/T} + 1}. \quad (5)$$

In order to ensure charge neutrality, the average number of electrons N_{elec} within the Wigner-Seitz sphere,

$$N_{\text{elec}} = \int_{r \leq r_s} d^3r \rho(\mathbf{r}, T), \quad (6)$$

is fixed to the atomic number Z . Then we obtain μ by solving the following equation:

$$Z - \sum_p \left(\int_{r \leq r_s} d^3r |\psi_p(\mathbf{r})|^2 \right) \tilde{n}_p(\mu, T) = 0. \quad (7)$$

With the chemical potential μ obtained from Eq. (7) one can construct $\rho(\mathbf{r}, T)$ from Eq. (4). Using $\rho(\mathbf{r}, T)$, the new updated atomic potential is obtained from Eq. (2). Afterwards, orbitals $\psi_p(\mathbf{r})$ and orbital energies ε_p are calculated from Eq. (3) using the new potential, and then a new μ is calculated. Equations (2) to (7) are repeated until convergence is reached. Thus, orbitals and orbital energies are determined self-consistently. In our calculations the

input parameters are the atomic number Z , the solid density via the Wigner-Seitz radius r_s , and the temperature T of the system.

After completing an average-atom calculation, one obtains the zeroth-order total energy within the Wigner-Seitz sphere (i.e., the total energy per atom),

$$E(T) = \sum_p \varepsilon_p \tilde{n}_p(\mu, T) \int_{r \leq r_s} d^3r |\psi_p(\mathbf{r})|^2. \quad (8)$$

Within the grand-canonical ensemble, one can calculate the probability distribution of all possible electronic configurations. If we consider a fixed bound-electron configuration $[n_b] = (n_1, \dots, n_B)$, where B is the number of bound one-electron (spin-orbital) states, then the probability distribution at temperature T is given by

$$P_{[n_b]}(T) = \prod_b^{\text{bound}} \frac{e^{-(\varepsilon_b - \mu)n_b/T}}{1 + e^{-(\varepsilon_b - \mu)/T}}, \quad (9)$$

where b runs over all bound states ($1 \leq b \leq B$) and n_b is an integer occupation number (0 or 1) in the bound-electron configuration. Then the charge-state distribution is given by

$$P_Q(T) = \sum_{[n_b]}^Q P_{[n_b]}(T), \quad (10)$$

where $[n_b]$ runs over all possible bound-state configurations satisfying $\sum_b^{\text{bound}} n_b = Z - Q$.

III. RESULTS AND DISCUSSION

In our study we consider a system consisting of carbon atoms. For a reasonable comparison of the results from the two methods, one should choose a system that can be addressed using both tools. AA does not consider any motion of atomic nuclei. Therefore we had to restrict the translational motion of atoms and atomic ions in XMDYN simulations as well. In order to do so, we set the carbon mass artificially so large that atomic movements were negligible throughout the calculations. Further, we increased the carbon-carbon distances to reduce the effect of the neighboring ions on the atomic electron binding energies. In XMDYN simulations, we chose a super-cell of 512 carbon atoms arranged in a diamond structure, but with a 13.16 Å lattice constant (in case of diamond it is 3.567 Å). The number density of the carbon atoms is $\rho_o = 3.5 \times 10^{-3} \text{Å}^{-3}$ which corresponds to a mass density of 0.07g/cm³. Plasma was generated by choosing different irradiation conditions typical at

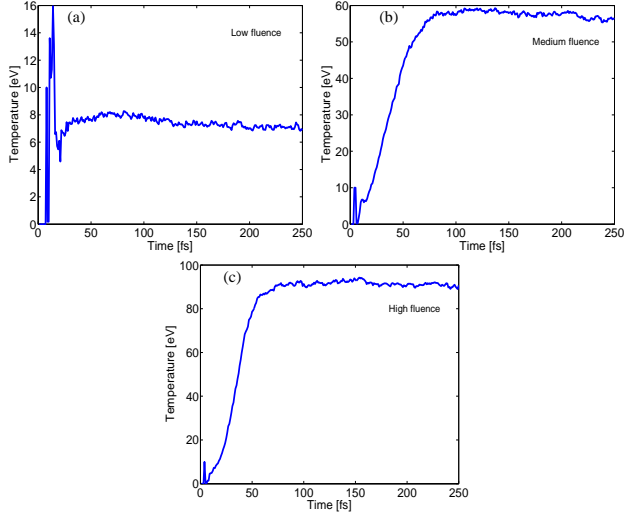


FIG. 1. Time evolution of the temperature of the plasma within XMDYN simulation during and after x-ray irradiation at different fluences: (a) $\mathcal{F}_{\text{low}} = 6.7 \times 10^9 \text{ ph}/\mu\text{m}^2$, (b) $\mathcal{F}_{\text{med}} = 1.9 \times 10^{11} \text{ ph}/\mu\text{m}^2$ and (c) $\mathcal{F}_{\text{high}} = 3.8 \times 10^{11} \text{ ph}/\mu\text{m}^2$. In all three cases, the pulse duration is 10 fs FWHM; the pulse is centered at 20 fs, and the photon energy is 1 keV. Note that in all cases equilibrium is reached within 100 fs after the pulse.

XFELs. Three different fluences, $\mathcal{F}_{\text{low}} = 6.7 \times 10^9 \text{ ph}/\mu\text{m}^2$, $\mathcal{F}_{\text{med}} = 1.9 \times 10^{11} \text{ ph}/\mu\text{m}^2$, and $\mathcal{F}_{\text{high}} = 3.8 \times 10^{11} \text{ ph}/\mu\text{m}^2$ were considered. In all three cases the photon energy and pulse duration were 1 keV and 10 fs (full width half maximum), respectively. From XMDYN plasma simulations shown in Fig. 1, the time evolution of the temperature of the plasma is analyzed by fitting to Eq. (1). Counterintuitively, right after photon absorption has finished, the temperature is still low, and then it gradually increases although no more energy is pumped into the system. The reason is that during the few tens of femtoseconds irradiation the fast photoelectrons are not yet part of the thermal distribution; initially only the low-energy secondary electrons and Auger electrons that have lost a significant part of their energy in collisions determine the temperature. The fast electrons thermalize on longer timescales as shown in Figs. 1(b) and (c), contributing to the equilibrated subset of electrons. In all cases equilibrium is reached within 100 fs after the pulse.

AA calculates only the equilibrium properties of the system, which means that it does not consider the history of the system's evolution through non-equilibrium states. We first calculate the total energy per atom, $E(T)$, Eq. (9), as a function of temperature T within a carbon system of density ρ_o . In this way we obtain a relation between the average energy

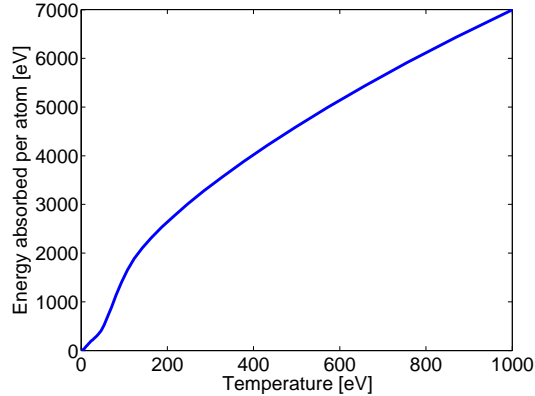


FIG. 2. Relation between plasma temperature and energy absorbed per atom in AA calculations for a carbon system of mass density $0.07\text{g}/\text{cm}^3$.

Parameters	Low fluence	Medium fluence	High fluence
Fluence ($\text{ph}/\mu\text{m}^2$)	6.7×10^9	1.9×10^{11}	3.8×10^{11}
Energy absorbed per atom (eV)	29	665	1170
XMDYN temperature (eV)	7	57	91
AA temperature (eV)	6	60	83

TABLE I. Final temperatures obtained from XMDYN runs after 250 fs propagation and from AA calculations. XMDYN temperatures are obtained from fitting using Eq. (1), while AA temperatures are obtained from the absorbed energy–temperature relation (Fig. 2).

absorbed per atom, $\Delta E = E(T) - E(0)$, and the electron temperature (see Fig. 2). In XMDYN simulation the average number of photoionization events per atom, n_{ph} , is available for each fluence point, and therefore the energy absorbed on average by an atom is known ($= n_{\text{ph}} \times \omega_{\text{ph}}$, where ω_{ph} is the photon energy). Using this value we can select the corresponding temperature that AA yields. This temperature is compared with that fitted from XMDYN simulation. All these results are in reasonable agreement, as shown in Table I. Later we use this temperature for calculating the charge-state distributions.

Figure 3 represents the kinetic-energy distribution of the electron plasma (in the left panels) and the charge-state distributions (in the right panels) for the three different fluences. The charge-state distributions obtained from XMDYN at the final timestep (250 fs) are compared to those obtained from AA at the temperatures specified in Table I. Although similar charge states are populated using the two approaches, differences can be observed:

AA yields consistently higher ionic charges than XMDYN, (20%-30% higher average charges) for the cases investigated.

This is probably for the following reasons. XMDYN calls XATOM on the fly to calculate re-optimized orbitals for each electronic configuration. In this way XMDYN accounts for the fact that ionizing an ion of charge Q costs less energy than ionizing an ion of charge $Q+1$. However, in the current implementation of AA, this effect is not considered. At a given temperature, AA uses the same orbitals (and, therefore, the same orbital energies) irrespective of the charge state. A likely consequence is that AA gives more population to higher charge states, simply because their binding energies are underestimated. That could also be the reason why AA produces wider charge-state distributions and predicts a somewhat higher average charge than XMDYN does. The other reason for the discrepancies could be the fact that XMDYN treats only those orbitals as being quantized that are occupied in the ground state of the neutral atom. For carbon, these are the $1s$, $2s$, and $2p$ orbitals. All states above are treated classically in XMDYN, resulting in a continuum of bound states. As a consequence, the density of states is different and it may yield different orbital populations and therefore different charge-state distributions. In spite of the discrepancies observed, XMDYN and AA equilibrium properties are in reasonably good agreement.

We also performed simulations under the conditions that had been used in a recent publication using a continuum approach [16]. A Gaussian x-ray pulse of 10 fs FWHM was used. The intensities considered lie within the regime typically used for high-energy-density experiments : $I_{\max} = 10^{16} \text{ W/cm}^2$ for $\omega_{\text{ph}} = 1000 \text{ eV}$, and $I_{\max} = 10^{18} \text{ W/cm}^2$ for $\omega_{\text{ph}} = 5000 \text{ eV}$. We employed a super-cell of diamond (mass density = 3.51 g/cm^3) containing 1000 carbon atoms within the PBC framework. In this study, 25 different Monte-Carlo realizations were calculated and averaged for each irradiation case in order to improve the statistics of the results. The average energy absorbed per atom [Fig. 5] is $\sim 28 \text{ eV}$ and $\sim 26 \text{ eV}$, respectively, for the 1000-eV and 5000-eV photon-energy cases, in agreement with Ref. [16]. Figure 4 shows the time evolution of the average charge for two different photon energies. Average atomic charge states of +1.1 and +0.9, respectively, were obtained long after the pulse was over. Although the rapid increase of the average ion charge is happening on very similar times, the charge values at the end of the calculation are 30% and 40% higher than those in Ref. [16] for the 1000-eV and 5000-eV cases, respectively [Fig. 4(a,b)].

We can name two reasons that can cause such differences in the final charge states. One

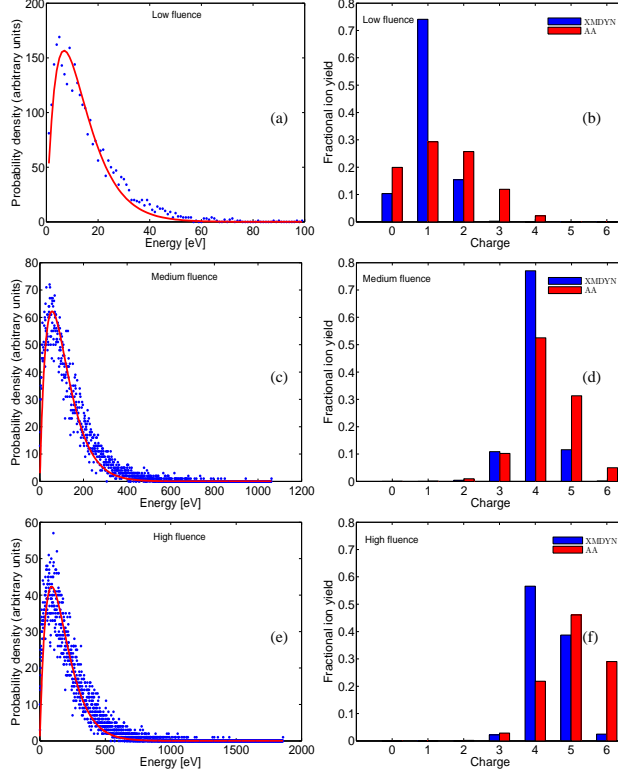


FIG. 3. Kinetic-energy distribution of the electron plasma and charge-state distributions from AA and XMDYN simulations (250 fs after the irradiation) for the low fluence (a,b), the medium fluence (c,d), and the high fluence (e,f).

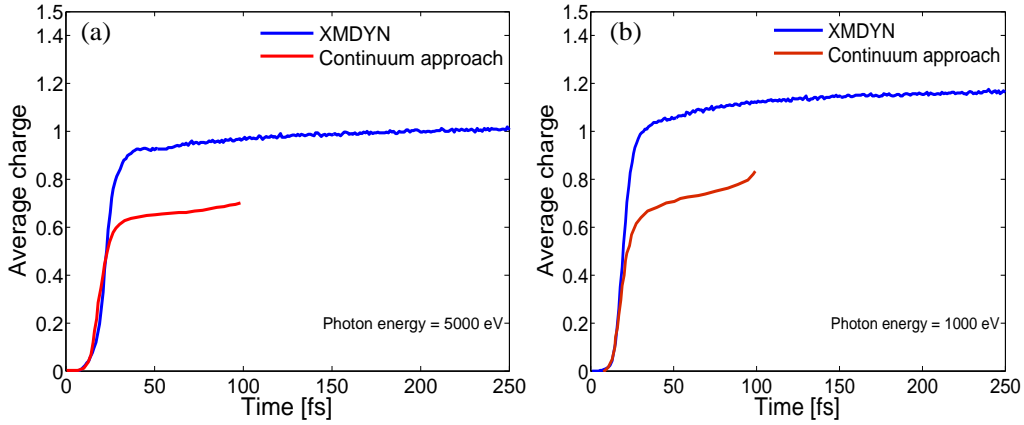


FIG. 4. (a,b) average charge within diamond irradiated with a Gaussian pulse of hard and soft x rays of $\omega_{\text{ph}} = 5000$ eV, $I_{\text{max}} = 10^{18}$ W/cm² and $\omega_{\text{ph}} = 1000$ eV, $I_{\text{max}} = 10^{16}$ W/cm², respectively. In both cases, a pulse duration of 10 fs FWHM was used.

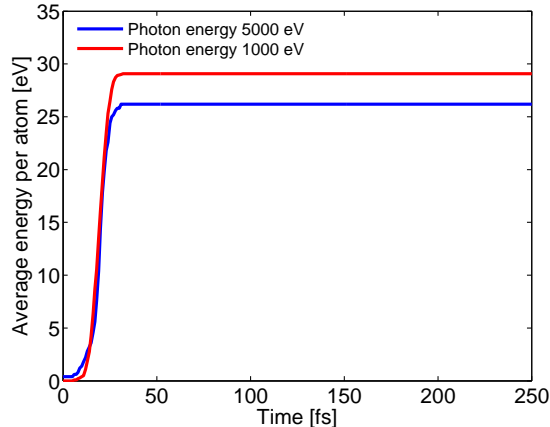


FIG. 5. Average energy absorbed per atom within diamond irradiated with a Gaussian pulse of hard and soft x rays of $\omega_{\text{ph}} = 5000$ eV, $I_{\text{max}} = 10^{18}$ W/cm² and $\omega_{\text{ph}} = 1000$ eV, $I_{\text{max}} = 10^{16}$ W/cm², respectively. In both cases, a pulse duration of 10 fs FWHM was used.

is that two different formulas for the total impact ionization cross section were used in the two approaches. In Ref. [16] the cross sections are approximated from experimental ground state atomic and ionic data [34] while XMDYN employs the semi-empirical BEB formula. Figure 6(a) compares these cross sections of neutral carbon atom. It can be seen that cross section and, therefore, the rate of the ionization used by XMDYN are larger, which can shift the final average charge state higher as well. The second reason is the evaluation of the three-body recombination cross section. In Ref. [16] recombination is defined using the principle of microscopic reversibility which states that the cross-section of impact ionization can be used to calculate the recombination rate [35]. In the current implementation of the Boltzmann code the two-body distribution function is approximated using one-body distribution functions in the evaluation of the rate for three-body recombination, whereas in XMDYN correlations at all levels are naturally captured within the classical framework due to the explicit calculation of the microscopic electronic fields. Beside the fundamental differences in the two approaches one can see a good agreement between the final average charge states.

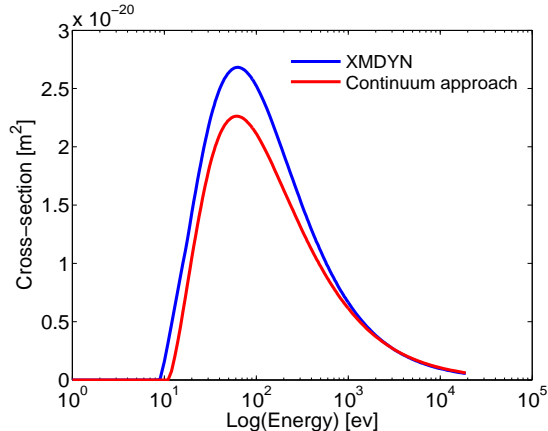


FIG. 6. Comparison of impact ionization cross sections for neutral ground-state carbon used in the current work within XMDYN based on the BEB formula [32], and the cross sections used in the continuum approach of Ref. [16] based on experimental data.

IV. CONCLUSIONS

We have investigated the thermalization dynamics of x-ray-heated carbon systems using the simulation tool XMDYN and compared its predictions to two other conceptually different simulation methods, the average-atom model (AA) and the Boltzmann continuum approach. Both XMDYN and AA are naturally capable to address ions with arbitrary electronic configurations, a very common situation in high-energy-density matter generated by, e.g., high-intensity x-ray irradiation. We found very similar temperatures for thermalized model systems calculated with the two methods. Qualitative agreement can be observed between the predicted ion charge-state distributions, although AA tends to yield somewhat higher charges. The reason could be that in the current implementation, AA uses fixed atomic binding energies irrespective of the atomic electron configuration. We also compared results from XMDYN and the Boltzmann continuum approach for the thermalization dynamics of XFEL-irradiated diamond. Thermal equilibrium of the electron plasma is reached within similar times in the two descriptions, although the asymptotic average ion charge states are somewhat different. The discrepancy could be attributed to the different approaches towards impact ionization and recombination processes in the two models and to different parametrizations used in the simulation. In this paper we have considered only light atomic species such as carbon. However, there is no restriction in XMDYN to consider

heavy atomic ions with any electronic configuration. Therefore, with XMDYN the treatment of systems including heavy atomic species (exhibiting complex inner-shell relaxation pathways) will be more comprehensive and therefore may be more reliable. Finally, we note that, in contrast to a Boltzmann continuum approach, it is straightforward within XMDYN to treat spatially inhomogeneous systems consisting of several atomic species.

ACKNOWLEDGEMENT

We thank Beata Ziaja for fruitful discussions. This work has been supported by the excellence cluster “The Hamburg Center for Ultrafast Imaging (CUI): Structure, Dynamics and Control of Matter at the Atomic Scale” of the Deutsche Forschungsgemeinschaft.

-
- [1] C. Pellegrini, A. Marinelli, and S. Reiche, *Rev. Mod. Phys.* **88**, 015006 (2016).
 - [2] C. Bostedt *et al.*, *Rev. Mod. Phys.* **88**, 015007 (2016).
 - [3] L. Young *et al.*, *Nature* **466**, 56 (2010).
 - [4] S. M. Vinko *et al.*, *Nature* **482**, 59 (2012).
 - [5] U. Zastraub *et al.*, *Phys. Rev. E* **90**, 013104 (2014).
 - [6] A. Lévy *et al.*, *Phys. Plasmas* **22**, 030703 (2015).
 - [7] B. Murphy, Z. Jurek, *et al.*, *Nat. Commun.* **5**, 4281 (2014).
 - [8] T. Tachibana, Z. Jurek, *et al.*, *Scientific Reports* **5**, 10977 (2015).
 - [9] S. P. Hau-Riege, R. A. London, and A. Szoke, *Phys. Rev. E* **69**, 051906 (2004).
 - [10] B. Ziaja, A. de Castro, E. Weckert, and T. Möller, *Eur. Phys. J. D* **40**, 465 (2006).
 - [11] O. Peyrusse, *Phys. Rev. E* **86**, 036403 (2012).
 - [12] B. Rudek *et al.*, *Nature Photon.* **6**, 858 (2012).
 - [13] H. Fukuzawa *et al.*, *Phys. Rev. Lett.* **110**, 173005 (2013).
 - [14] H.-K. Chung, M. H. Chen, W. L. Morgan, Y. Ralchenko, and R. W. Lee, *High Energy Density Phys.* **1**, 3 (2005).
 - [15] H.-K. Chung, M. H. Chen, W. L. Morgan, and Y. Ralchenko, *J. Quant. Spectrosc. Radiat. Transfer* **38**, 131 (1987).

- [16] B. Ziaja, V. Saxena, S.-K. Son, N. Medvedev, B. Barbrel, B. Woloncewicz, and M. Stransky, Phys. Rev. E **93**, 053210 (2016).
- [17] H. A. Scott, J. Quant. Spectrosc. Radiat. Transfer **71**, 689 (2001).
- [18] M. Bergh, N. Timneanu, and D. van der Spoel, Phys. Rev. E **70** (2004).
- [19] Z. Jurek, G. Faigel, and M. Tegze, Eur. Phys. J. D **29**, 217 (2004).
- [20] C. Gnodtke, U. Saalman, and J. M. Rost, Phys. Rev. A **79**, 041201(R) (2009).
- [21] C. Caleman *et al.*, J. Mod. Opt. **58**, 1486 (2011).
- [22] S. P. Hau-Riege, Phys. Rev. Lett. **108**, 238101 (2012).
- [23] L. Fang *et al.*, Phys. Rev. Lett. **109**, 263001 (2012).
- [24] Z. Jurek, S.-K. Son, B. Ziaja, and R. Santra, J. Appl. Cryst. **49**, 1048 (2016).
- [25] S.-K. Son, R. Thiele, Z. Jurek, B. Ziaja, and R. Santra, Phys. Rev. X **4**, 031004 (2014).
- [26] N. Rohringer and R. Santra, Phys. Rev. A **76**, 033416 (2007).
- [27] S.-K. Son, L. Young, and R. Santra, Phys. Rev. A **83**, 033402 (2011).
- [28] S.-K. Son and R. Santra, Phys. Rev. A **85**, 063415 (2012).
- [29] M. M. Abdullah, Z. Jurek, S.-K. Son, and R. Santra, J. Phys. Conf. Ser. **635**, 102008 (2015).
- [30] M. M. Abdullah *et al.*, Struct. Dyn. **3**, 054101 (2016).
- [31] N. Metropolis *et al.*, J. Chem. Phys. **21**, 1087 (1953).
- [32] Y.-K. Kim and M. E. Rudd, Phys. Rev. A **50**, 3954 (1994).
- [33] I. Georgescu, U. Saalman, and J. M. Rost, Phys. Rev. A **76** (2007).
- [34] M. A. Lennon *et al.*, J. Phys. Chem. Ref. Data **17**, 1285 (1988).
- [35] V. Saxena and B. Ziaja, Physics of Plasmas **23**, 012710 (2016).